Results in Physics 10 (2018) 903–912

Contents lists available at ScienceDirect

Results in Physics

journal homepage: www.elsevier.com/locate/rinp

Rapid fabrication of a lightweight 2 m reaction-bonded SiC aspherical mirror

Longxiang Li[a,b,*], Zhenyu Liu[a,b], Donglin Xue[a,b,*], Weijie Deng[a,b], Ruigang Li[a,b], Yang Bai[a,b], Xuefeng Zeng[a,b], Xuejun Zhang[a,b]

[a] Key Laboratory of Optical System Advanced Manufacturing Technology, Chinese Academy of Sciences, Changchun 130033, China
[b] Changchun Institute of Optics, Fine Mechanics and Physics, Chinese Academy of Sciences, Changchun, Jilin 130033, China

ARTICLE INFO

Keywords:
Computer controlled polishing
Silicon carbide mirror
Surface error
Magnetorheological finishing
Large polishing lap

ABSTRACT

Magnetorheological finishing (MRF) fabrication can effectively facilitate a rapid fabrication of an aspherical 2 m reaction-bonded silicon carbide mirror. The dwell-time algorithm and tool path supported tool-mark mitigation and virtual-axis employment are analyzed. A rapid-fabrication strategy alternates MRF and a large polishing lap to converge surface error profile before MRF alone is used to high-precise finishing. In the alternate-use process, large polishing lap's dwell time map for low-order space frequency is calculated before MRF's for high-order one, but executed later in reality. The fabricated mirror with a silicon modification layer showed accuracy convergence from 0.098 λ rms to 0.019 λ rms at 84.6 h, demonstrating the strategy's validity for large optical-surface processing.

Introduction

Rapidly developing high-resolution modern optical technology has required increasing the primary-mirror apertures in large optical-telescope systems. Some of the large mirrors are monolithic, including Large Binocular Telescope (LBT)'s 8.4 m primary mirror [1], Very Large Telescope (VLT)'s 8.2 m primary mirror [2], Subaru Telescope's 8.2 m primary mirror [3], Gemini south/north telescope's 8.1 m primary mirror [4], Multiple Mirror Telescope's 6.5 m primary mirror [5], Hale Telescope's 5.08 m primary mirror [6], Southern Astrophysical Research (SOAR) telescope's 4.1 m primary mirror [7], Space Surveillance Telescope (SST)'s 3.5 m primary mirror [8], Hubble Space Telescope's 2.4 m primary mirror [9] and other many monolithic large mirrors. Some of the large mirrors are segmented, including the typical European Extremely Large Telescope (E-ELT)'s 39.3 m primary mirror segmented by 798 hexagonal 1.4 m mirrors [10], Thirty Meter Telescope (TMT)'s 30 m primary mirror segmented by 492 hexagonal 1.4 m off-axis aspherics [11], Giant Magellan Telescope (GMT)'s 24.5 m primary mirror segmented by seven 8.4 m diameter mirrors [12], Keck Telescope's 10 m primary mirror segmented by thirty-six 1.8 m mirrors [13], James Webb Space Telescope (JWST)'s 6.5 m primary mirror segmented by eight-teen mirrors [14] and so on.

The materials of most of the large mirror mentioned above are mainly Zerodur, ULE or Borosilicate [15–17]. But Silicon carbide (SiC) has been judged one of the best materials available for space-borne optical mirrors because of its outstanding thermal and mechanical properties [18,19]. As an example, SiC is used as the material of the 3.5 m primary mirror of Herschel Space Observatory [18]. Reaction-bonded SiC (RB-SiC) as one kind of SiC material, which is easily configured for large apertures, requires a silicon-modification-layer coating because the roughness of the two-phase RB-SiC surface complicates production of a highly polished surface. Fabrication difficulties arising with large-aperture light-weight RB-SiC aspherical mirrors include canceling quilting errors, achieving high-precision surface profiles, and lowering the time and cost of fabrication. The typical sub-aperture fabricating methods include Computer Controlled Optical Surfacing (CCOS) [20], Stressed Lap (SL) [21], active lap polishing [22], Magnetorheological Finishing (MRF) [23], Ion Beam Figuring (IBF) [24] and so on. With such techniques used, small and medium size SiC mirrors are fabricated well today. However, fabrication of large aperture SiC mirror or extremely large SiC mirrors, are rarely reported.

Decreases in the determinacy of fabrication of large-aperture aspherical mirrors that follow the measurement of the accuracy of the surface-error profile to λ/10 (λ = 632.8 nm) would be achieved with conventional polishing processes using such materials as pitch or polyurethane pads because of variations in pad material, polishing abrasive, slurry properties, temperature, equipment type, and setup [25]. Thus, fabrication typically enters a highly iterative, low-

* Corresponding authors at: Changchun Institute of Optics, Fine Mechanics and Physics, Chinese Academy of Sciences, Changchun, Jilin 130033, China.
E-mail addresses: lilx@ciomp.ac.cn (L. Li), xuedl@ciomp.ac.cn (D. Xue).

https://doi.org/10.1016/j.rinp.2018.08.013
Received 27 May 2018; Received in revised form 6 August 2018; Accepted 6 August 2018
Available online 10 August 2018

convergence process of testing and polishing. Further, this polishing process, which depends on the application of normal forces, can easily cause mechanical defects in lightweight mirrors constructed with a honeycomb-core structure. These defects may take the form of quilting errors on the mirror's optical surface [26].

Magnetorheological (MR) finishing (MRF) is a typical, deterministic sub-aperture figuring and polishing technology [27–30]. Its polishing tool conforms well to the optical surface and presents no mismatch problems between the tool and parts. The circulating MR fluid ensures that the MRF's polishing tool incurs no wear and leads to MRF exhibiting a stable removal function (influence function) during the polishing process. This performance maintains the high convergence efficiency of the optical-surface error. Further, the advantages of MRF also include subsurface damage reductions and fine surface roughness. QED, having done an excellent job in MRF, built a large MRF machine called Q22-2000F that owns a 2.5 m mirror fabrication capability [26]. A team from National University of Defense Technology in China built a 2 m MRF machine as well [31]. But large mirrors, especially SiC mirrors up to or large than 2 m size, were rarely reported publicly fabricated by MRF. MRF presents challenges that must be overcome before it can be used to polish a lightweight 2 m RB-SiC aspherical mirror.

This paper presents the rapid convergence of a lightweight 2 m RB-SiC aspherical mirror's surface error at the beginning of λ/10 root mean square (rms). The use of the dwell-time algorithm and tool path to mitigate tool marks and employment of the virtual axis are discussed. Then, a rapid-fabrication strategy is followed to fabricate an aspherical 2 m mirror. Finally, the project-used 2 m RB-SiC mirror with a silicon modification layer is fabricated to demonstrate the utility of this technique.

Experimental setup

Five-axis computer numerical control machine

The working wheel of the MRF module has a diameter of 360 mm with a permanent magnet. Fig. 1 shows its main components: cycle system, nozzle, permanent magnet, working wheel, recycle device, and other electrical control systems. The parameters in the cycle system that require controlled stability are viscosity, temperature, and flow of the MR fluid.

The base computer numerical control (CNC) machine includes three linear axes—*X*, *Y*, and *Z*—and two rotational axes—*A* and *C*. The arrangement of these axes is shown in Fig. 1(b). Axis *A* rotates around axis *X*, and axis *C*, representing the working table, rotates around axis *Z*. The rotational axes of an MRF wheel or a conventional polishing pad can be added to this base CNC machine. The maximum diameter of producible mirrors is 2.5 m

Dwell-time algorithm

MRF inherits its basic subaperture-polishing characteristics from the general computer-controlled optical-surfacing (CCOS) system [32,33]. The dwell-time algorithm is based on the principle that the desired amount of optical material to be removed is determined by a convolution operation of the dwell time and removal function

$$E(x, y) = r(x, y) ** T(x, y) \tag{1}$$

where $E(x,y)$ is the distribution of the desired amount of material to be removed from the optical surface, $r(x,y)$ is the removal function or influence function, $T(x,y)$ is the dwell-time distribution at the dwell points on the tool path, and ** indicates the algebraic expression for a two-dimensional convolution operation. Directly treating the convolution in MRF using Eq. (1) is difficult. For example, the angle of the D-shape MRF removal function relative to a certain coordinate axis is variable when the MRF polishing tool dwells at different points on the spiral polishing path. The conventional deconvolution methods for circular symmetrical removal functions—the Fourier transform and iterative convolution strategy—are not applicable to this situation in MRF.

The linear matrix equation

$$Rt = e, \begin{cases} t \geqslant \sigma \\ \sigma > 0 \end{cases} \tag{2}$$

can be transferred from the convolution operation to solve the dwell-time distribution in MRF by considering the subaperture figuring process [34,35]. This expression includes several values: **R** is the matrix related to the removal function, data points on the initial surface-error profile, and dwell points on the tool path; **e** is the row vector presenting the initial surface-error map on the optical surface; **t** is the row vector presenting the period of dwell time distributed at different dwell points; and **σ** is the positive constraint on the dwell time.

Eq. (2) is a typical algebraic linear-inverse problem with a positive constraint. One valid method for solving this equation uses the positive dwell-time algorithm in [36]. This algorithm is fast enough to obtain the dwell-time distribution of the 2 m mirror by MRF with highly accurate determinations of the residual surface error.

This dwell-time computing strategy based on the linear-matrix conduct operation rather than the convolution offers many advantages. It may be applied to almost any type of path over which the MRF polishing tool scans, and the space density of the dwell points or surface-error-map points can be set to any desired value. Moreover, this strategy provides the possibility that variant removal functions or different types of scanning paths may be used in the same fabricating process.

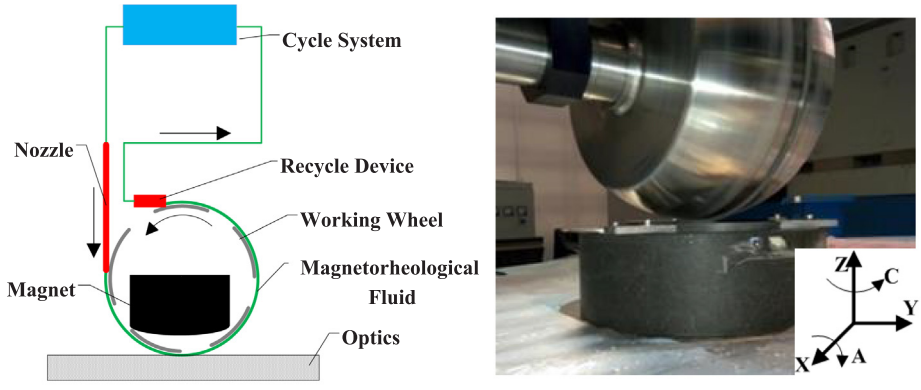

Fig. 1. MRF device. (a) Component nomenclature and arrangement. (b) MRF working wheel.

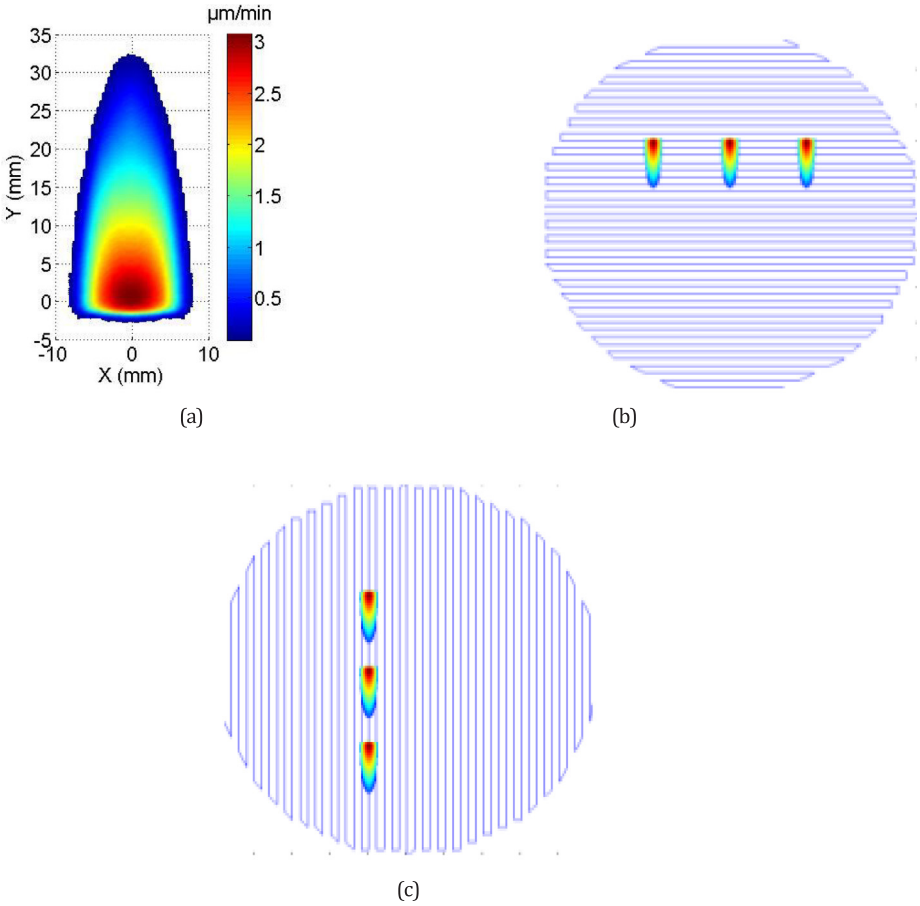

Fig. 2. Removal function and its scanning directions along raster paths. (a) Removal function. (b) Scan along the *X* axis. (c) Scan along the *Y* axis.

Tool path

The fabrication process for a 2 m aspherical surface employs the usual raster path. However, MRF requires the consideration of two factors: tool-mark errors on the large-aperture optical surface and the attitude control of the MRF's polishing tool in the CNC machine.

Mitigation of tool marks

Tool-mark errors are always present in subaperture polishing technologies. The tool marks from MRF are more obvious on the optical surface because MRF is a deterministic polishing technology. Tool marks are related to several parameters in the polishing process, including the distribution of the removal function, depth of removal material, and tool-path step size [37–39]. We found that an important parameter, the scanning direction of the MRF removal function, cannot be ignored.

Fig. 2(a) shows a typical removal function of MRF. The removed material is Si. The rotating speed of the wheel is 60 r/min. The polishing distance, that is the gap between the working wheel and the mirror, is 2 mm. The polishing powder is diamond with 1 μm diameter. The temperature of magnetorheological fluid is set to 20 °C. The removal rate distribution of the MRF removal function, unlike removal functions from ion-beam figuring or other technologies that show circular symmetry, differs in the *X* and *Y* directions. These two scanning directions of the removal function on the tool path are shown in Fig. 2(b) and (c).

These tool marks can be simulated on a uniform material-removal layer of the optical surface. Fig. 3(a) and (b) show simulations in which the thickness of the uniform material-removal layer was 1000 nm, and the raster-path step size was 3 mm. Then, the depths of the simulated tool-mark errors were 50.33 nm and 8.21 nm for scans in the *X* and *Y* directions, respectively. Therefore, MRF polishing of the 2 m aspherical RB-SiC mirror uses the scanning direction shown in Fig. 2(c) with a 3 mm raster-path step size.

Virtual rotational axis

One attitude-control principle for the MRF process requires that the normal direction of the outer surface of the MRF working wheel is aligned with the normal direction of the local aspherical surface. This principle is illustrated in Fig. 4(a) and (b). Even though the MR fluid can be attached to a large region of the working wheel, its effective working region depends on the area of the magnet field. In practice, as Fig. 4(b) shows, the usual attitude control is oriented so that the direction of line BA is collinear to the normal direction of the local optical surface. That is, a CNC machine used for MRF needs at least two rotational axes to determine a raster path on a curved surface. This requirement increases the cost and complexity of using a CNC machine in MRF. Obviously, the CNC machine illustrated in Fig. 1 does not possess two rotational axes for the attitude control of an MRF working wheel for manufacturing an aspherical 2 m mirror.

A virtual rotational axis is therefore used in the MRF process to overcome the problem just described [40,41]. One may take into account the effective region of the magnet and the size of the removal function by noting that any points in the area between arc CD on the working wheel can replace point A as the point nearest to the optical surface. Fig. 4(c) illustrates this arrangement and the area between arc CD is the effective virual-axis working region. In this case, one of the two rotational axes mentioned above is no longer necessary. Thus, the

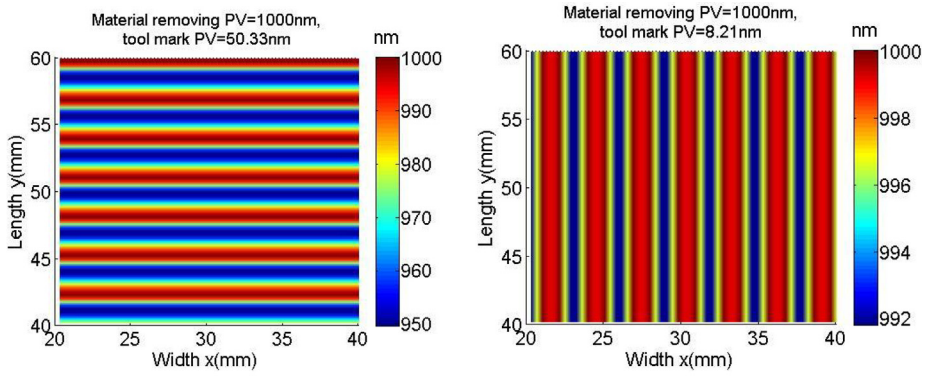

Fig. 3. Simulation of tool marks for different scanning directions. (a) Scanning in the *X* direction. (b) Scanning in the *Y* direction.

cost and complexity of the CNC machine used for MRF both decrease.

The use of the virtual rotational axis requires that the magnet is designed and optimized to keep the removal function the same as before. This constraint then requires that the removal function should be the same as that of point A no matter which point along arc CD in Fig. 4(c) is used as the point nearest to the optical surface.

experimental mirror with material matching the material in the 2 m RB-SiC mirror. The results appear in Fig. 5(b). The placement of the 0° value of θ shown in Fig. 4(a) determines that the point nearest to the optical surface is point A. Then, the maximum angle of the virtual rotational axis provided by the magnet field falls within ± 15°. Fig. 5(c) shows that the variations of the peak-to-valley (PV) and volume removal rate of the removal function along the virtual rotational axis remain near 3%. This performance is sufficiently stable to support polishing aspherical large-aperture mirrors.

Figuring procedures

Using only one polishing or figuring technology to obtain high accuracy of the surface profile at high material removal rates with low

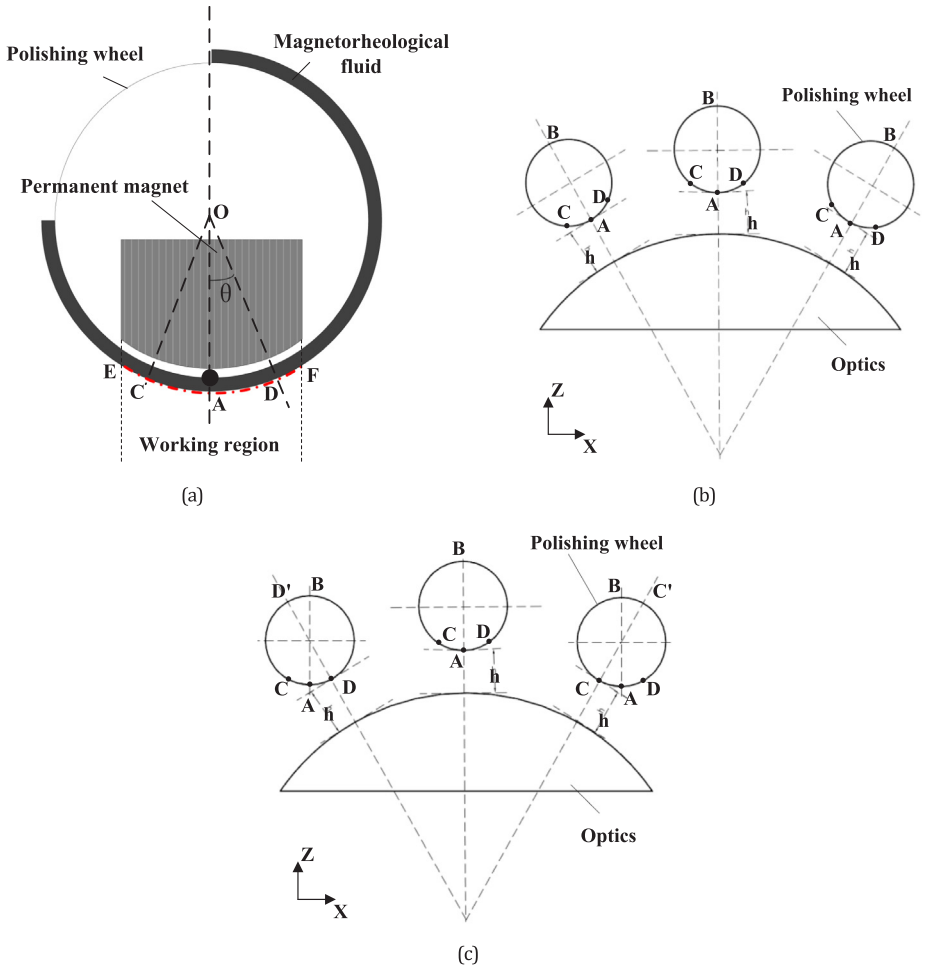

Fig. 4. Attitude control of the MRF polishing tool. (a) Effective working region of the MR fluid on the wheel surface. (b) Attitude control along the real rotational axis. (c) Attitude control along the virtual rotational axis.

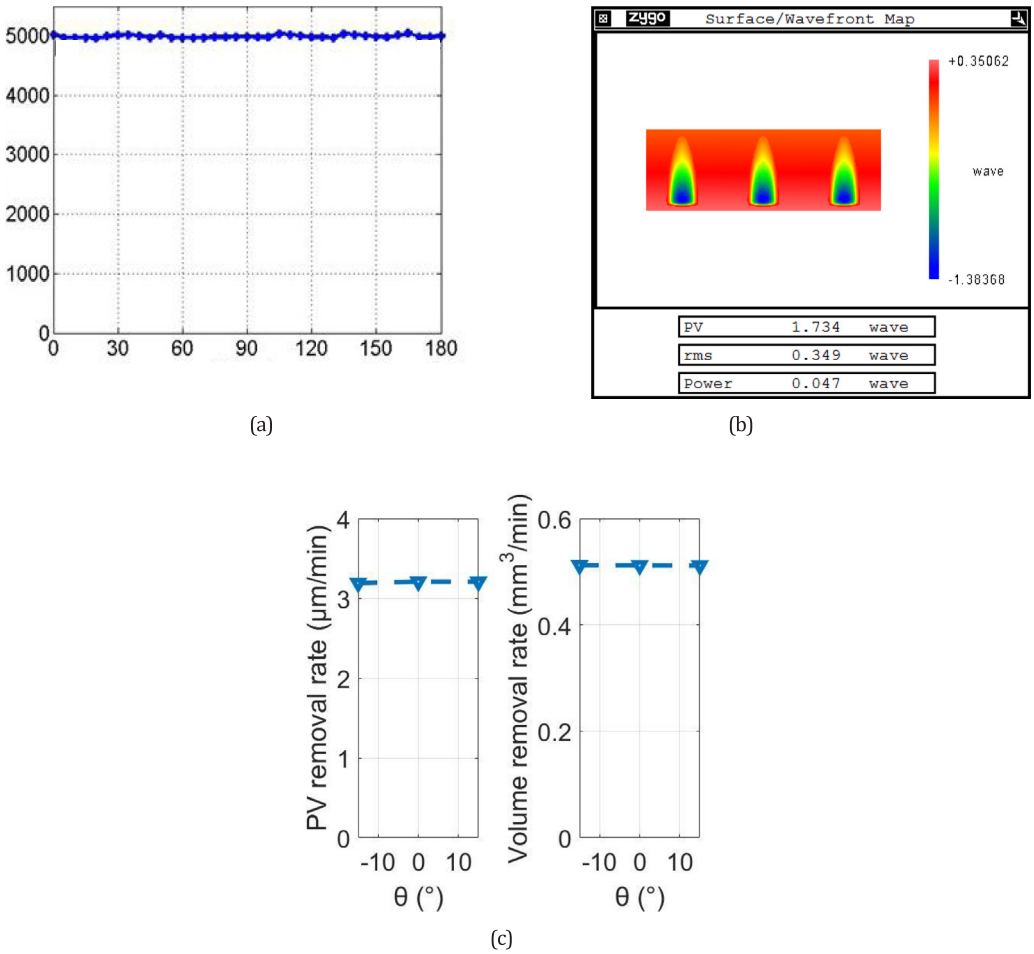

Fig. 5. Virtual rotational axis of the working wheel. (a) Magnetic field distribution. (b) Surface maps after 20 s for values of θ of -15°, 0°, and $+15^{\circ}$, from left to right, respectively. (c) Variations in PV and volume removal rate of the removal function.

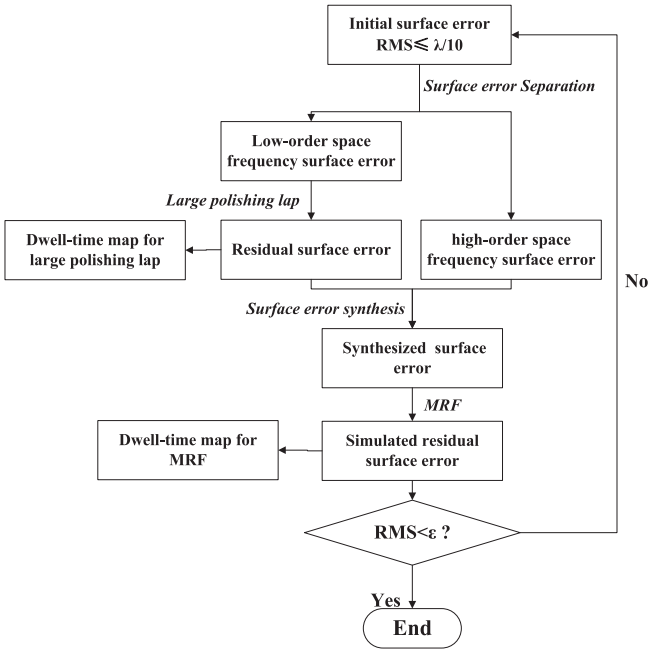

Fig. 6. Flowchart of dwell-time map calculation in the alternate-use process.

iterative-convergence processes is almost impossible in producing 2 m aspherical optics. This paper presents the introduction to the fabricating process of both a large polishing lap as a conventional polishing process and MRF. These additions to the proposed technique occur after the rms of the 2 m optical material was decreased to λ/10. First, the large polishing lap and MRF were used alternately to produce highly accurate polishing of the initial surface with some remaining error. Then, MRF was used alone to converge the surface error to the desired level.

Alternate-use of large polishing lap and MRF

For the dwell-time map calculation in the alternate-use process that produces dwell-time maps and predicts polishing results, the initial surface-error map is separated initially into low-order and high-order space frequency parts. The Zernike polynomial is employed to separate the initial surface error according to space frequencies. Thus,

$$E_{\mathrm{ini}} = E_{low} + E_{high} \tag{3}$$

and

$$E_{\mathrm{low}} = \sum_{\mathrm{i}}^{N} C_i \times Z_i, \tag{4}$$

where E_{ini} is the initial surface-error map, E_{low} is the low-order space frequency-error map fitted by the Zernike polynomial in Eq. (4), N is the number of the Zernike polynomial, E_{high} represents the high-order space frequency-error map, which is the residual part after the initial surface error is fitted by the Zernike polynomial, and Ci is the polynomial coefficient.

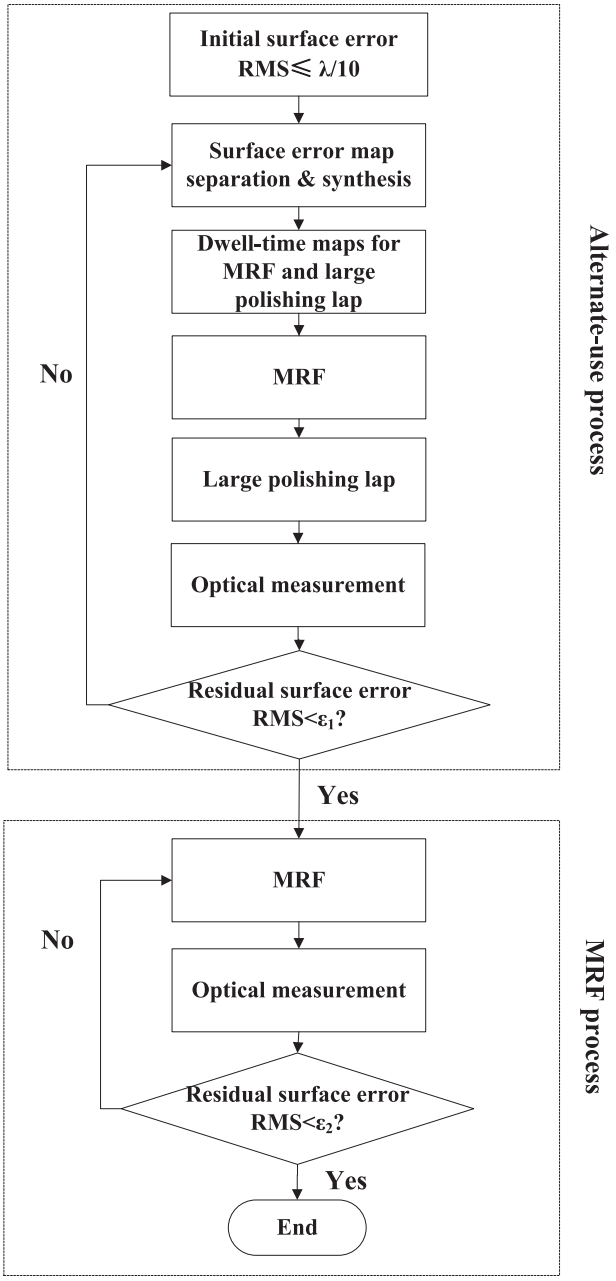

Fig. 7. Flowchart of the real fabrication process.

Fig. 6 shows that the large polishing lap is used first to correct low-order space frequency-surface errors arising from the dwell-time map calculation of the alternate-use process. Then, the residual surface error from the large polishing lap and E_{high} are synthesized together. MRF, in this approach will correct the synthesized error map virtually. The dwell-time maps for the large polishing lap and MRF are both obtained from the process depicted in the flowchart in Fig. 6. Even though the dwell-time map of the large polishing lap is calculated first, the large polishing lap is carried out after MRF in real fabrication. This ordering takes into account the capacity of the large polishing lap to smooth out tool marks of MRF as shown in the real alternate-use process outlined in Fig. 7.

Final surface-error-correction with MRF

Fig. 7 shows that when the accuracy of the surface-error map approaches ε_1, which usually falls in the range of λ/30 to λ/40, the 2 m mirror enters the domain of the high-precision figuring process by using MRF alone. In this stage, the large polishing lap is not readily available to achieve higher accuracy by reducing the surface error because of its low determinacy in the polishing process. MRF, however, retains a high convergence rate. Moreover, the amount of residual removal material in this stage is small, yielding weak tool-mark errors from MRF. Therefore, MRF can provide effective convergence of the surface error to higher accuracy ε_2 through a low-iterative process with weak tool-mark errors.

Results and discussion

The mirror examined in this research project had a diameter of 2040 mm and was composed of a silicon modification layer on an RB-SiC substrate. This parabolic mirror had a clear aperture with a diameter of 2000 mm. The lightweight, honeycomb-core structure is illustrated in Fig. 8(a) [42,43]. Some of the basic process parameters for MRF and large polishing lap are shown in Tables 1 and 2.

After several iterative operations to perform testing and polishing on the silicon modification layer, the surface-error map mainly displayed quilting errors with rms 0.098 λ, as shown in Fig. 8(b). The presence of quilting errors is attributable to the dependence of a conventional polishing lap on a high normal pressure that causes mechanical defects in the mirror during its polishing. Fig. 8(b) presents the initial surface-error map and is the starting point for this paper's approach to the whole polishing or figuring process.

First, MRF was used to converge the initial surface-error map gradually to avoid risk to the 2 m mirror used in the project. This also permitted adjustments to the rate of the removal function for the next iterative process that followed the precorrection results of the surface-error map. Fig. 8(c) shows the 20 h real-fabrication process of the 2 m mirror by MRF, and Fig. 8(d) shows the result of this precorrection process. The rms of the surface error converged from 0.098 λ to 0.079 λ without the aspherical distortion correction in the optical metrology. The accuracy of the surface error obviously decreased to a small extent, which proves that MRF is capable of correcting the surface error of a 2 m mirror.

Next, the alternate-use of the large polishing lap with a diameter of 300 mm and MRF with the removal function sized to 16 mm × 35 mm was introduced. The step sizes of the path for MRF and the large polishing lap were 3 mm and 50 mm respectively. Fig. 7 presents the flowchart of the dwell-time map calculation process. The rms of the precorrection result shown in Fig. 8(d) was 0.077 λ after the aspherical distortion correction depicted in Fig. 9(a). Then, the surface-error-map separation was conducted using the first 36 terms of the Zernike polynomial. The low-order and high-order space-frequency surface-error maps are shown in Fig. 9(b) and (c), respectively. Then, in the dwell-time map calculation process, the low-order space-frequency surface-error map was converged using the large polishing lap; the result of this operation appears in Fig. 9(d). Here, the rms was 0.017 λ after polishing for 5.0 h. The synthesized surface-error map, as shown in Fig. 9(e), used data from Fig. 9(c) and (d). Finally, Fig. 9(f) presents the synthesized surface-error map figured by MRF through the virtual process of alternate-use of the large polishing lap and MRF. Although the virtual residual error can be calculated with higher accuracy than 0.014 λ rms by the dwell-time algorithm described in Section "Dwell-Time Algorithm", the total dwell time of MRF was kept to 41.3 h. The 0.014 λ rms demonstrated in this approach exceeded practical engineering requirements.

The real fabrication process that alternately uses the large polishing lap and MRF is shown in Fig. 7. Here, MRF is used first because the tool marks from MRF can be eliminated by the large polishing lap. The result of the process of alternate-use appears in Fig. 9(g) and (h); here, the rms values were 0.031 λ and 0.029 λ before and after the aspherical distortion correction, respectively.

Finally, the 2 m mirror was figured only by MRF, as shown in Fig. 8.

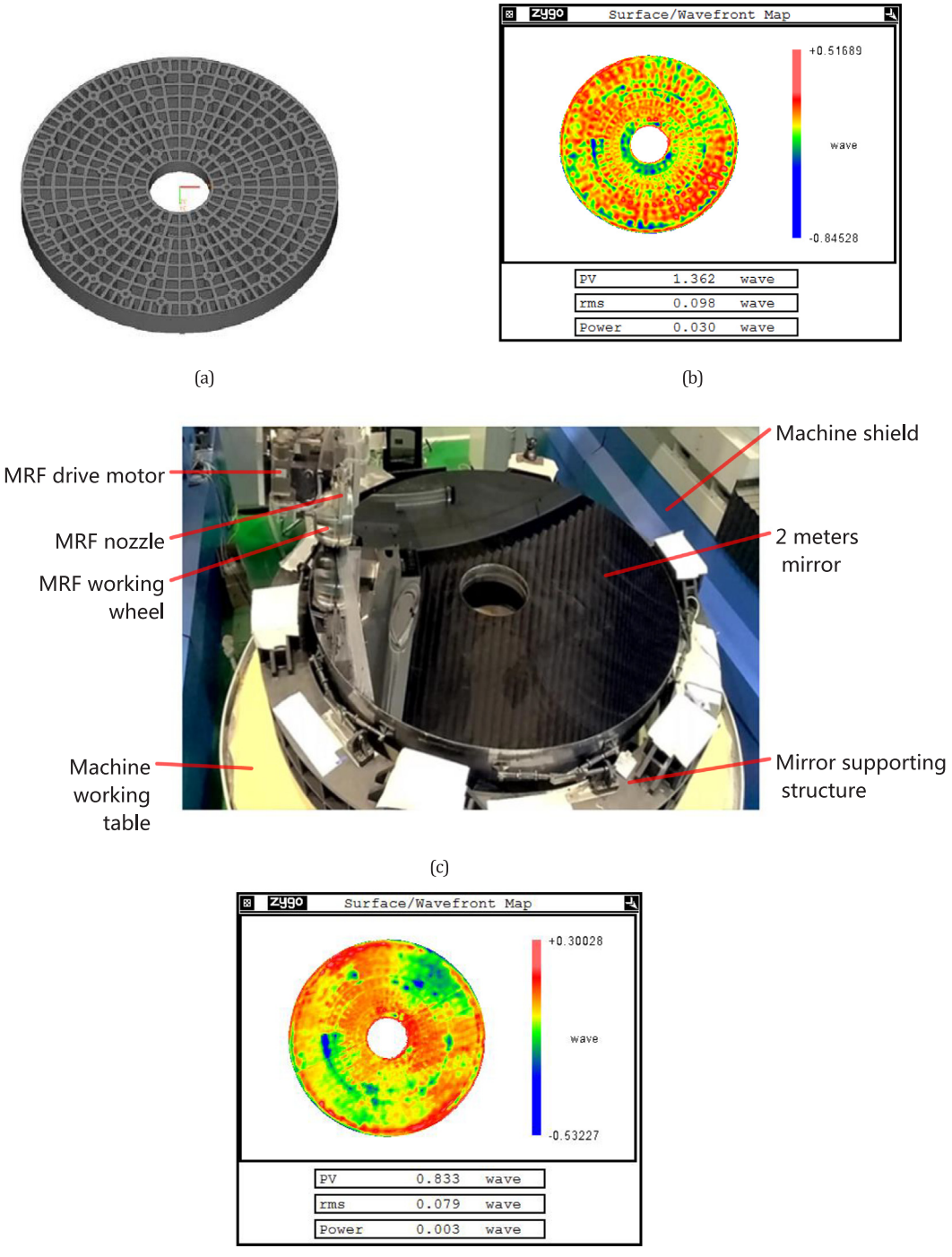

Fig. 8. 2 m mirror precorrection process. (a) Lightweight mirror structure. (b) Surface-error map after conventional polishing lap operation. (c) 2 m mirror polished by MRF. (d) Residual-error map after precorrection process with MRF.

Table 1
Basic process parameters used for MRF.

Parameter	Magnitude	unit
Rotating speed of the wheel	60	r/min
Maximum magnetic intensity	5000	Gs
Polishing distance	2	mm
Diamond powder diameter	1	μm
Temperature	20	℃
Feed step	3	mm
Removal function size	16 × 35	mm

Table 2
Basic process parameters used for large polishing lap.

Parameter	Magnitude	unit
Rotating speed of the lap	200	r/min
Cerium powder diameter	3	μm
Temperature	23	℃
Feed step	50	mm
Lap diameter	300	mm

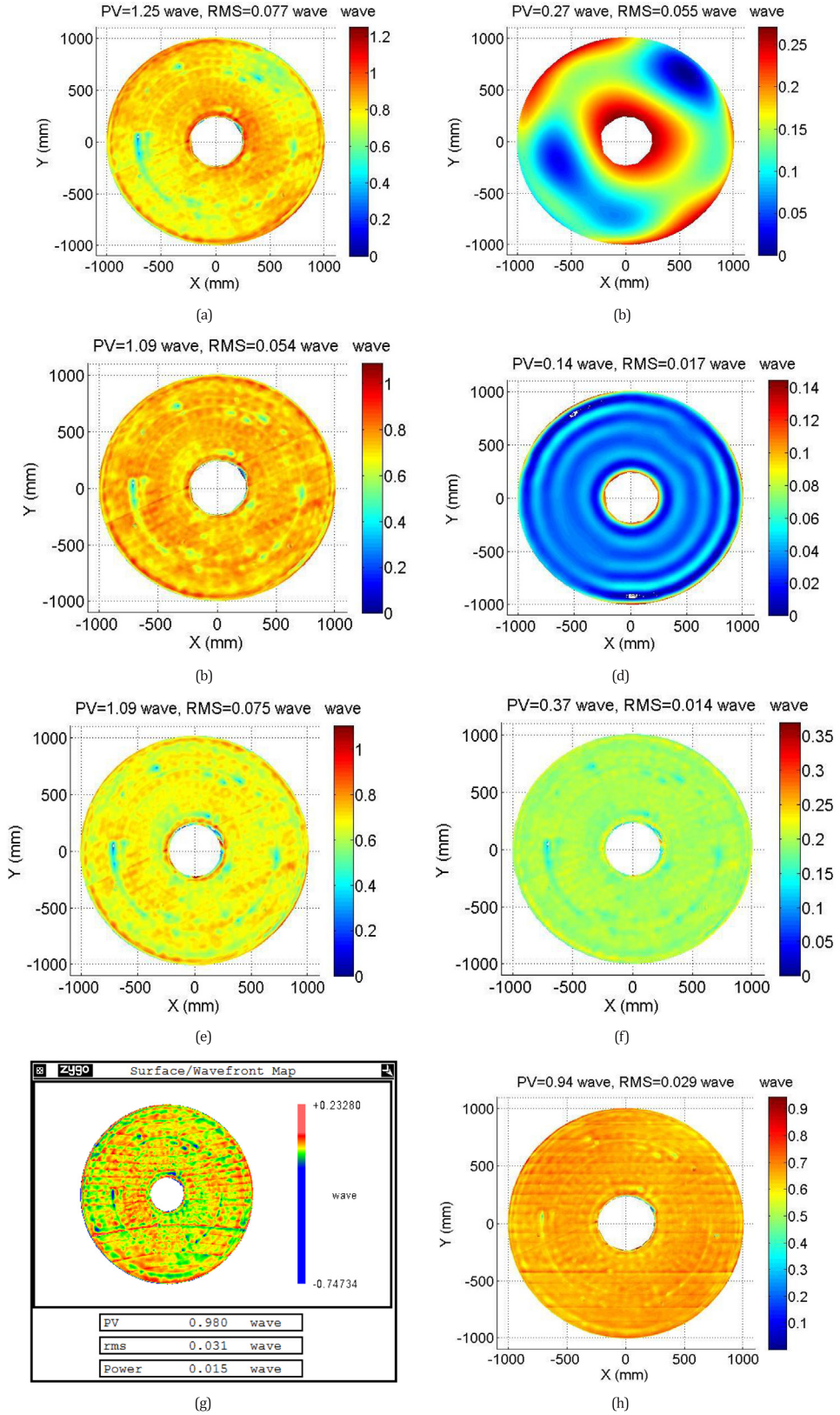

Fig. 9. Results from alternate-use of the large polishing lap and MRF. (a) Residual-error map after precorrection process with MRF, aspherical distortion correction applied. (b) Surface-error map of the low-order space frequency. (c) Surface-error map of the high-order space frequency. (d) Virtual residual-error map from the large polishing lap operation (e) Synthesized surface-error map for the dwell-time map calculation process. (f) Final virtual residual-surface-error map for MRF. (g) Final real surface-error map before the aspherical distortion correction. (h) Final real surface-error map after aspherical distortion correction.

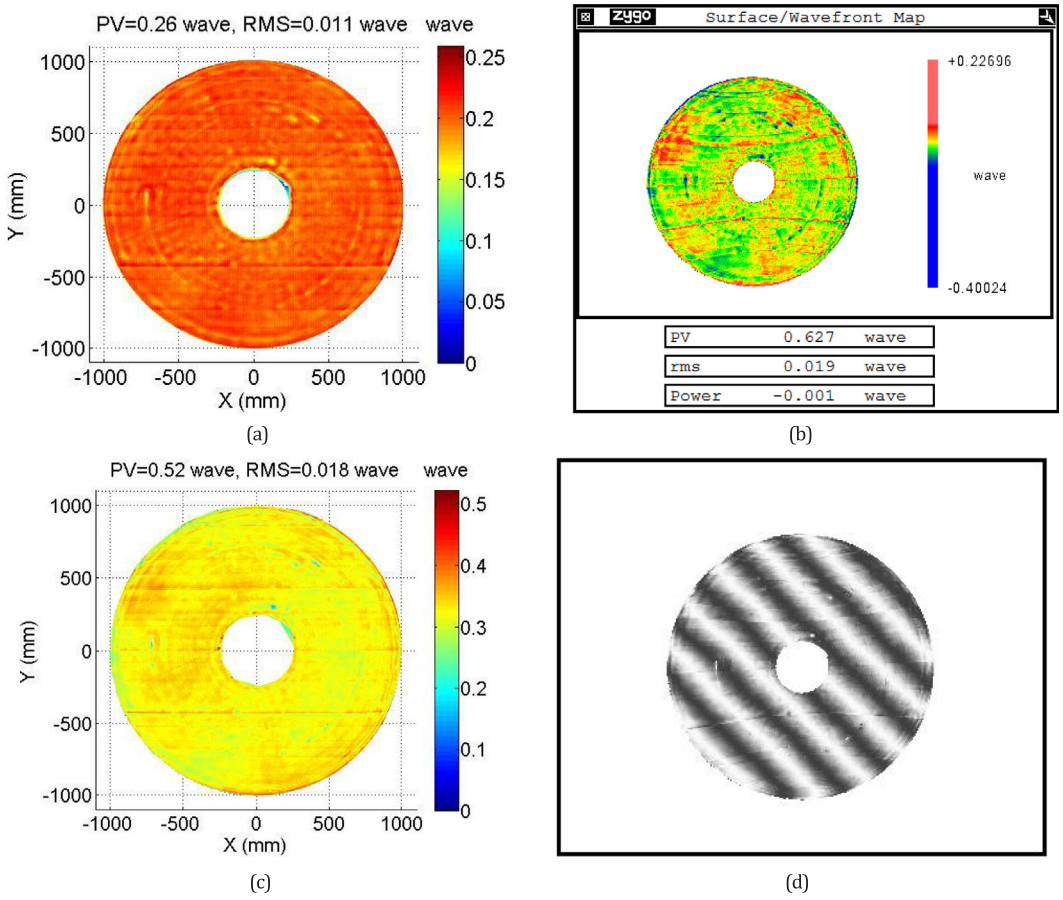

Fig. 10. Final surface error for the 2 m mirror prepared using only MRF. (a) Final virtual surface-error map. (b) Final real surface-error map. (c) Final real surface-error map after aspherical distortion correction. (d) Fringe map of the mirror surface following final MRF.

In this process, the desired amount of material removal became small, and the rms of the initial surface-error map was 0.029 λ, as shown in Fig. 9(h). Then, the corresponding rms of the virtual residual-surface-error map was 0.011 λ, as shown in Fig. 10(a). The final rms of the real surface-error map after performing MRF alone for 18.3 h was 0.019 λ, as shown in Fig. 10(b). The corresponding surface-error map with aspherical distortion correction was 0.018 λ, as shown in Fig. 10(c). Further, the fringe map of the final surface-error map of this 2 m SiC mirror appears in Fig. 10(d).

In this section, the whole polishing and figuring process for the 2 m aspherical mirror is presented. Starting with 0.098 λ rms of the initial surface error, it ended with 0.019 λ rms of the final surface error by three iterative processes of testing and polishing. The total elapsed time for polishing is 84.6 h as shown in Table 3.

In the second iterative process, by separating the surface error into high and low-order space frequency, large polishing lap's dwell time map for low-order space frequency is calculated before MRF's for high-order one, but executed later in reality. This strategy speeds up and promotes the convergence of the surface error of the 2 m mirror. The total elapsed polishing or figuring time of this process is 46.3 h including a 5.0 h large polishing lap and 79.6 h of MRF. In fact, if only large polishing lap was used to this process, the total elapsed time would be longer for the large polishing lap is hardly to figure relatively high-order space frequency whose space period is smaller than the size of the lap. Correspondingly if only MRF was used, the total elapsed time would be longer as well, because the rate of the MRF's removal rate is lower than large polishing lap who is suitable to low-order space frequency. Furthermore, in this process the tool marks error are also taken into account seriously, which leads that large polishing lap's dwell time calculated earlier but executed later. Therefore, alternate use of the MRF and large polishing lap in this process is an optimized strategy.

In the third iterative process, only MRF is used to figure the surface error of the 2 m mirror. Just 18.3 h is taken to converge the surface error from 0.031 λ rms to 0.019 λ rms. In this process, the determinacy of MRF is made full use of, although MRF's rate of material removal is lower than large polishing lap's. Therefore, while the desired amount of material removal became small and low order space frequency of surface error map does not dominate, Only using MRF can reach a goal to fast converge the surface error.

Table 3
presents the final data for the high-precision polishing and figuring process for this 2 m aspherical mirror.

	Technology	Map Accuracy rms (λ) Starting Surface Map	Virtual Surface Error	Real Surface Error	Elapsed Time (h)
1	MRF	0.098	0.068	0.079	20
2	Lap + MRF	0.079	0.014	0.031	5.0 + 41.3
3	MRF	0.031	0.011	0.019	18.3

Conclusions

Obtaining high-accuracy large-aperture optics is a great challenge for modern optical-fabrication technology. MRF, a typical subaperture optical-surfacing technology, was used here to fabricate a 2 m RB-SiC mirror. A rapid fabrication strategy for this 2 m mirror was devised using the proper dwell-time algorithm, a good tool path to mitigate tool marks, and the system's virtual axis.

In this strategy, large polishing lap's dwell time map for low-order space frequency is calculated before MRF's for high-order one, but executed later in reality. When the accuracy of the surface-error map is up to high levels, MRF was used alone to provide careful and high-precision figuring of the surface-error map.

A 2 m RB-SiC mirror with a silicon modification layer was fabricated to demonstrate the validity of this technique. The starting 0.098 λ rms of the initial surface-error map was converged to 0.019 λ. The total elapsed time was only 84.6 h, which included a 5.0 h large polishing lap and a 79.6 h MRF. Several points of conclusions follow.

a. MRF plays a crucial role in the fast convergence of the 2 m surface-error map from the starting point below λ/10 rms to λ/50 rms. Such a rate of convergence meets the requirements of a practical project.
b. The fabricating determinacy, which compares the real and virtual surface-error convergence rates, is between 60% and 75%, although the large polishing lap was used.
c. The large polishing lap, conducted after MRF in the process that employed alternate-use, not only smoothes the optical surface to reduce the tool marks from MRF but also converges the low-order space-frequency surface-error map. It is beneficial for the fabrication of a large-aperture optical surface.
d. This paper's strategy merits trials with lower-accuracy stages. For instance, this approach would remain valid if the rms of the initial surface profile took values up to λ/5.

The experimental results indicate the validity of the strategy presented in this paper for the fabrication of 2 m mirrors. The method and technique developed in this paper could be applied to the preparation of large optical surfaces.

Funding Information

We acknowledge National Natural Science Foundation of China (NSFC) (61605202) and Key research projects of Frontier Science of Chinese Academy of Science (QYZDJ-SSW-JSC038-02)

References

[1] Hill JM. The large binocular telescope. Appl. Opt. 2010;49:115–22.
[2] Luehe OVD, Derie F, Koehler B, Paresce F, D'Arcio L. Interferometry with the ESO Very Large Telescope. Proc. SPIE –Int. Soc. Opt. Eng. 1997;2566:9.
[3] Kaifu AN. SUBARU Telescope. Proc. SPIE 1998;15:14–22.
[4] Roy JR. The start of scientific observations with the gemini north telescope. Bull. Am. Astron. Soc. 2001.
[5] West SC, Callahan SP, Chaffee FH, Davison WB, Derigne ST, Fabricant DG, Foltz CB, Hill JM, Nagel RH, Poyner AD. Toward first light for the 6.5-m MMT telescope. Opt. Telescopes Today Tomorrow 1997:38–48.
[6] Kells W, Dressler A, Carr D, Koch E, Epps H, Pardeilhan G. 5 meter hale telescope prime focus. Publ. Astron. Soc. Pac. 1998;110.
[7] Warner M, Krabbendam V, Schumacher G. SOAR Telescope: 4-meter high-performance-mount performance results. Proc. SPIE –Int. Soc. Opt. Eng. 2004;5495:77–86.
[8] Woods DF. Space Surveillance Telescope: focus and alignment of a three mirror telescope. Opt. Eng. 2013;52:3604.
[9] Crocker JH. Fixing the hubble space telescope. Proc. SPIE –Int. Soc. Opt. Eng. 1991;22:2–8.
[10] Rees PCT, Gray C. Metrology requirements for the serial production of ELT primary mirror segments. SPIE Opt. Eng. + Appl. 2015:957508.
[11] Cole GC. Optical fabrication and metrology for the thirty meter telescope primary mirror segments. Opt. Fab. Test. 2017. pp. OW1B.4.
[12] Martin HM, Burge JH, Davis JM, Davison WB, Johns M, Kim DW, Su P, Zhou P. "Production of primary mirror segments for the Giant Magellan Telescope," in. SPIE Astronomical Telescopes + Instrumentation 2014:91510J.
[13] Vogt SS, Allen SL, Bigelow BC, Bresee L, Brown WE, Cantrall T, Conrad A, Couture M, Delaney C, Epps HW. "HIRES the high-resolution echelle spectrometer on the Keck 10-m Telescope," in Instrumentation in Astronomy. VIII 2005:362.
[14] Daukantas P, Carts Y. James Webb Space Telescope. Proc. Int. Astron. Union 2007;2:522–3.
[15] Jedamzik R. "ZERODUR progress in CTE characterization," in SPIE Optical Engineering +. Applications 2013:88600P.
[16] Vanbrocklin RR, Edwards MJ, Wells B. "Review of Corning's capabilities for ULE mirror blank manufacturing for an extremely large telescope," in Optomechanical Technologies. for Astronomy; 2006.
[17] Hill JM, Angel JRP. Proceedings of SPIE - The International Society for Optical Engineering 3352. 1998.
[18] Seo H, Han JY, Kim SW, Seong S, Yoon S, Lee K, Hong J, Lee H, Bok M. Novel orthogonal velocity polishing tool and its material removal characteristics from CVD SiC mirror surfaces. Opt. Express 2016;24:12349.
[19] Webb K. "Advances in fabrication technologies for light weight CVC SiC mirrors," in Optical Engineering +. Applications 2007:666606.
[20] Jones RA, Plante RL. Rapid Fabrication Of Large Aspheric Optics. Precis. Eng. 1986;9:65–70.
[21] Kim DW, Oh C, Lowman A, Smith GA, Burge JH. "Manufacturing of super-polished large aspheric/freeform optics," in Spie Astronomical Telescopes +. Instrumentation 2016:99120F.
[22] Walker DD, Bingham RG, Brooks D, Diego F, Humm B, Jamshidi H, Kim SW, Kim YS, Nixon G, Rees D. The Production of Highly Aspheric Secondary Mirrors Using Active Laps. Progress in Telescope & Instrumentation Technologies 1992;42:215.
[23] Golini D, Kordonski WI, Dumas P. Magnetorheological finishing (MRF) in commercial precision optics manufacturing. Proceedings of SPIE - The International Society for Optical Engineering 1999;3782:80–91.
[24] Schindler A. Ion beam figuring of SiC mirrors provides ultimate WFE performances for any type of telescope. Proceedings of SPIE - The International Society for Optical Engineering 1999;3739.
[25] Shorey AB, Kordonski W, Tricard M. Magnetorheological finishing of large and lightweight optics. Proc. SPIE 2004;5533:81–90.
[26] Hull T, Hartmann P, Clarkson AR, Barentine JM, Jedamzik R, Westerhoff T. Lightweight high-performance 1–4 meter class spaceborne mirrors: emerging technology for demanding spaceborne requirements. Proc. SPIE 2010;7739:327–30.
[27] Sidpara AM. Magnetorheological finishing: a perfect solution to nanofinishing requirements. Opt. Eng. 2014;53:092002.
[28] Żak Andrzej, Łaszcz Amadeusz, Hasiak Mariusz, Gerstein Gregory, Maier Hans Jürgen, Dudzinskic Wlodzimierz. Ion polishing as a method of imaging the magnetic structures in CoNiGa monocrystal. Results Phys. 2018(C):6277–80.
[29] Kheradmand S, Esmailian M, Fatahy A. A novel approach of magnetorheological abrasive fluid finishing with swirling-assisted inlet flow. Results Phys. 2016;6(C):568–80.
[30] Das M, Jain VK, Ghoshdastidar PS. Nanofinishing of flat workpieces using rotational–magnetorheological abrasive flow finishing (R-MRAFF) process. Int. J. Adv. Manuf. Technol. 2012;62.1-4:405–20.
[31] Li SY, Dai YF, et al. New Technology for Manufacturing and Measurement of Large and Middle-Scale Aspheric Surfaces. China National Defense Industry Press; 2011.
[32] Jones Wiktor RA, Rupp J. Rapid optical fabrication with computer-controlled optical surfacing. Opt. Photonics News 1991;30(12):1962–8.
[33] Schinhaerl Markus. Advanced techniques for computer-controlled polishing. SPIE 2008;7060. 70600Q1-70600Q12.
[34] Li L, Zheng L, Deng W, Wang X, Wang X, Zhang B, Bai Y, Hu H, Zhang X. Optimized dwell time algorithm in magnetorheological finishing. Int. J. Adv. Manuf. Technol. 2015;81:833–41.
[35] Drueding TW, Bifano TG, Fawcett SC. Contouring algorithm for ion figuring. Precis. Eng. 1995;17:10–21.
[36] Li L, Xue D, Deng W, Wang X, Bai Y, Zhang F, Zhang X. Positive dwell time algorithm with minimum equal extra material removal in deterministic optical surfacing technology. Appl. Opt. 2017;56:9098–104.
[37] Hu H, Dai Y, Peng X. Restraint of tool path ripple based on surface error distribution and process parameters in deterministic finishing. Opt. Express 2010;18:22973–81.
[38] Takizawa K, Beaucamp A. Comparison of tool feed influence in CNC polishing between a novel circular-random path and other pseudo-random paths. Opt. Express 2017;25:22411–24.
[39] Dunn CR, Walker DD. Pseudo-random tool paths for CNC sub-aperture polishing and other applications. Opt. Express 2008;16:18942.
[40] Messner W, Hall C, Dumas P, Hallock B, Tricard M, O'Donohue S, Miller S. Manufacturing meter-scale aspheric optics. Proc. SPIE 2007;6671:667106–8.
[41] Song C, Dai Y, Peng X. Magnetorheological finishing of low-gradient curved surfaces based on four-axis linkage technique. J. Cent. S. Univ. 2013;20:2349–58.
[42] Liu Z, Li L, Zeng X, Luo X, Zhang X. Fabrication of large aspheric mirror using multi-mode polishing based on error separation. Opt. Precis. Eng. 2017;25:813–9.
[43] L. Fan, Research on the lightweight design and support of the 2m-Si C primary mirror for ground-based telescope (Doctor Dissertation). (2013) (in Chinese).